

Associated Atmospheric Mechanisms for the Increased Cold Season Precipitation over the Three-River Headwaters Region from the Late 1980s^{clip}

SHASHA SHANG,^{a,b} GAOFENG ZHU,^a JIANHUI WEI,^b YAN LI,^c KUN ZHANG,^d RUOLIN LI,^{e,f} JOËL ARNAULT,^b ZHENYU ZHANG,^b PATRICK LAUX,^{b,g} QIANYA YANG,^h NINGPENG DONG,ⁱ LU GAO,^j AND HARALD KUNSTMANN^{b,g}

^a Key Laboratory of Western China's Environmental Systems (Ministry of Education), College of Earth and Environmental Sciences, Lanzhou University, Lanzhou, China

^b Institute of Meteorology and Climate Research (IMK-IFU), Karlsruhe Institute of Technology, Garmisch-Partenkirchen, Germany

^c Key Laboratory of Arid Climate Change and Reduction of Gansu Province, College of Atmospheric Sciences, Lanzhou University, Lanzhou, China

^d National Tibetan Plateau Data Center, Institute of Tibetan Plateau Research, Chinese Academy of Sciences, Beijing, China

^e Key Laboratory of Ecohydrology of Inland River Basins, Northwest Institute of Eco-Environment and Resources, Chinese Academy of Sciences, Lanzhou, China

^f Qilian Mountains Eco-Environment Research Center in Gansu Province, Lanzhou, China

^g Institute of Geography, University of Augsburg, Augsburg, Germany

^h State Key Laboratory of Hydrology-Water Resources and Hydraulic Engineering, College of Hydrology and Water Resources, Hohai University, Nanjing, China

ⁱ Department of Water Resources, China Institute of Water Resources and Hydropower Research, Beijing, China

^j Institute of Geography, Fujian Normal University, Fuzhou, China

(Manuscript received 28 January 2021, in final form 9 July 2021)

ABSTRACT: Precipitation in the Three-River Headwater (TRH) region has undergone significant changes as a result of global warming, which can affect water resources in downstream regions of Asia. However, the underlying mechanisms of the precipitation variability during the cold season (October–April) are still not fully understood. In this study, the daily China gridded precipitation product CN05.1 as well as the NCEP–NCAR reanalysis are used to investigate the characteristics of the cold season precipitation variability over the TRH region and associated atmospheric mechanisms. The cold season precipitation shows an increasing trend ($5.5 \text{ mm decade}^{-1}$) from 1961 to 2014, with a dry-to-wet shift in around the late 1980s. The results indicate that the increased precipitation is associated with the enhanced easterly anomalies over the Tibetan Plateau (TP) and enhanced southeasterly water vapor transport. The enhanced Walker circulations, caused by the gradients of sea surface temperature between the equatorial central-eastern Pacific and Indo-western Pacific in tropical oceans, resulted in strengthened easterly anomalies over the TP and the westward expansion of the anticyclone in the western North Pacific. Meanwhile, the changed Walker circulation is accompanied by a strengthened local Hadley circulation, which leads to enhanced meridional water vapor transport from tropical oceans and the South China Sea toward the TRH region. Furthermore, the strengthened East Asia subtropical westerly jet may contribute to the enhanced divergence at upper levels and anomalous ascending motion above the TRH region, leading to more precipitation.

KEYWORDS: Precipitation; Atmospheric circulation; Teleconnections; Sea surface temperature

1. Introduction

It is acknowledged that the warming rate in high-mountain regions is higher than that in lowland regions (Pepin et al. 2015; Pepin and Lundquist 2008; Rangwala and Miller 2012). Evidence from observations and modeling studies over high-altitude mountainous regions (Nijssen et al. 2001; Beniston 2003; Rangwala et al. 2009) has shown that this rapid warming can significantly accelerate changes of the hydrological cycle, especially precipitation, and thereby can modify water resources and ecosystems in downstream regions (Liu et al. 2011; de

Oliveira et al. 2017; Xi et al. 2018). This is particularly the case for the Three-River Headwater (TRH) region (Jiang and Zhang 2016), which is located in the hinterland of the Earth's "third pole," the Tibetan Plateau (TP) (Liu et al. 2009; Liu and Chen 2000; Qin et al. 2009).

The TRH region is the headwater region of three major rivers in East Asia (i.e., the Yangtze River, the Yellow River, and the Mekong River) with a mean annual runoff of about $500 \times 10^8 \text{ m}^3$ (Shao et al. 2017; Zhang et al. 2012). Precipitation in this region plays an important role in sustaining water in river systems (Jiang et al. 2017; Zhang et al. 2013) and maintaining biodiversity in ecosystems (Jiang and Zhang 2016). In particular, the high-altitude, mountainous TRH region is dominated by glaciers, snow cover, permafrost, and wetlands (L. Tong et al. 2014), which are highly vulnerable to global warming (Liu et al. 2014; Yao et al. 2012; Zheng et al. 2018). It has been reported that the warming rate ($0.3^\circ\text{C decade}^{-1}$) in the TP including the TRH region from 1975 to 2010 is more than twice as high as the global mean warming rate ($0.12^\circ\text{C decade}^{-1}$)

Supplemental information related to this paper is available at the Journals Online website: <https://doi.org/10.1175/JCLI-D-21-0077.s1>.

Corresponding authors: Gaofeng Zhu, zhugf@lzu.edu.cn; Jianhui Wei, jianhui.wei@kit.edu

(Chen et al. 2014; Rangwala and Miller 2012). At the seasonal scale, the 2-m air temperature in winter over this region has the highest increase and the value reaches up to $0.6^{\circ}\text{C decade}^{-1}$ for the minimum temperatures (You et al. 2016). The amplified warming climate has enhanced the variability and uncertainty of the precipitation (Liang et al. 2013; Yi et al. 2013; K. Tong et al. 2014). Consequently, the increased variability and uncertainty in the precipitation has been propagated to various hydrological components through their nonlinear interactions in the study region (Jiang and Zhang 2016; Li et al. 2013; L. Tong et al. 2014; Xu et al. 2016, 2018; Zhang et al. 2012; Zhu et al. 2015)—for example, the expansion of wetlands, the shrinking of desert, and the recovery of the ecosystem environment due to the warmer and wetter climate (Zhu et al. 2015; Jiang and Zhang 2016). Therefore, the understanding of changed precipitation characteristics and underlying mechanisms over the TRH region is fundamental for achieving the water-related sustainable development goals of the country (Li et al. 2012).

Precipitation variability is usually affected by moisture supply, large-scale atmospheric circulations, and some local factors (Gustafsson et al. 2010; Chen and Avissar 1994). Studies show that the water precipitated in the TRH region originated mainly from the tropical Indian Ocean, the Bay of Bengal, and the North Atlantic (Simmonds et al. 1999; X. Xu et al. 2008). The variation of precipitation is impacted by changes in large-scale atmospheric circulations (Cuo et al. 2013; Liu and Yin 2001; Ma et al. 2018; Wang et al. 2017). For example, the precipitation variability in the southern TP region is affected by the North Atlantic Oscillation (NAO) (Wang et al. 2017) and El Niño–Southern Oscillation (ENSO) (Shaman and Tziperman 2005). The sea surface temperature (SST) anomalies in the Indian Ocean and the Atlantic Ocean (Hu and Duan 2015; Gao et al. 2013) exert strong effects on the precipitation variability over the TP. Moreover, the formation of precipitation over the TP is generally related to convection induced by thermodynamic and dynamic processes (Sugimoto and Ueno 2010). Specifically, given the high elevation of the TP, thermodynamic processes (e.g., surface sensible heating) are enhanced by the larger amount of the incoming solar radiation compared to those over lowland regions (Yanai and Tomita 1998; Boos and Kuang 2010). The surface heating–induced ascent of air lifts moisture from the low-level boundary layer up to the high-level free troposphere and contributes to the formation of convective precipitation (Sugimoto and Ueno 2010).

Previous studies have made significant progress in understanding the precipitation variability in the TP and indicate that the climate of the TP has regional features and remarkable seasonal changes (Yang et al. 2014; Liu and Yin 2001; Z. Xu et al. 2008; Wang and Guo 2012; Guo and Wang 2014). The precipitation over the TRH region in spring and winter increased remarkably from 1961 onward (Shi et al. 2016; Yi et al. 2013; K. Tong et al. 2014). The main focus of research, however, was on the moisture budget and mechanisms of the summer precipitation variation in this region during the recent 30 years (from 1979 onward) (Sun and Wang 2019; Wang et al. 2017; Sun and Wang 2018; Dong et al. 2020). Nevertheless, few studies shed light on the responsible water vapor transport and atmospheric mechanisms for the changed precipitation in the

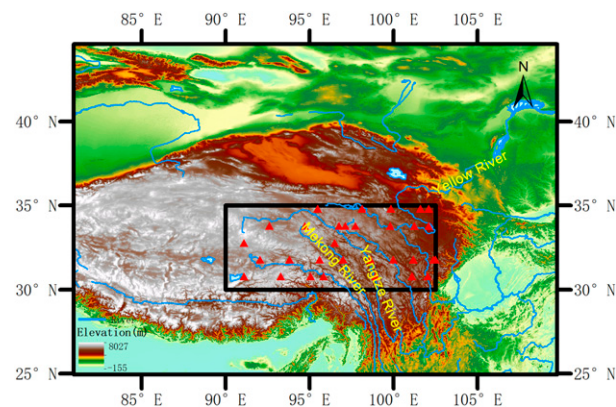


FIG. 1. Geographical overview of the Three River Headwater (TRH) region. The area within the black box depicts the study region. The red triangles denote the locations of the meteorological stations. The blue solid lines indicate the rivers in the TRH and its surrounding regions.

cold season (including spring and winter) from 1961 onward. Besides, in the context of global warming, the cold season precipitation variation is important as the strongest warming occurs in cold season, which leads to changes in the energy and water balance at the land surface (Wang et al. 2019; Zhao et al. 2007). Changes in soil moisture and snow cover have been reported in numerous studies (e.g., Wang et al. 2002; Wu and Zhang 2008; You et al. 2020; Bai et al. 2019). Furthermore, the precipitation and the modified freeze-thaw processes in soils during the cold season have strong impacts on the productivity of plants during the upcoming growing season (such as in alpine meadow areas), which eventually affects the economic development of the region (Fu et al. 2018; Kang et al. 2010; Shen et al. 2011).

Therefore, this study aims to improve the understanding of the variation of the cold season (October to April) precipitation over the TRH region from 1961 to 2014 and the underlying atmospheric mechanisms. The research questions addressed are the following:

- 1) What are the spatial and temporal variabilities of the cold season precipitation over the TRH region?
- 2) What are the related water vapor transport and atmospheric mechanisms responsible for the variability of the cold season precipitation?

2. Datasets and methods

a. Datasets

In this study, the analyzed TRH region is defined as a rectangular area (30° – 35°N , 90° – 102.5°E ; black rectangle in Fig. 1), and the analyzed cold season is defined as the period from October to next April (Yao et al. 2012) for the period from 1961 to 2014. To analyze the precipitation variability over the TRH region, four long-term precipitation datasets are used in this study: the daily CN05.1 data and station data from the National Meteorological Information Center of the China

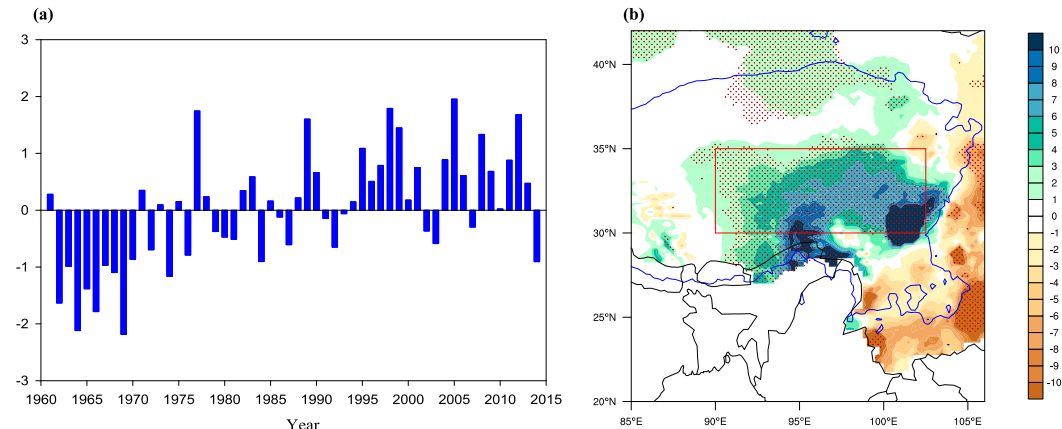


FIG. 2. (a) Time series of the standardized cold season precipitation (nondimensional), averaged over the TRH region. (b) Spatial pattern of the linear trend in the cold season precipitation (mm decade^{-1}) for the TRH and its surrounding regions from 1961 to 2014. Superimposed red dots in (b) indicate that the areas where the linear trend in the cold season precipitation is statistically significant at the 95% confidence level. The curved blue lines delineate the 2000-m isohyposes.

Meteorological Administration, the monthly Global Precipitation Climatology Center (GPCC) data (Schneider et al. 2016), and the monthly Climatic Research Unit Time Series (CRU) data (Harris et al. 2014). The long-term daily CN05.1 product is derived from daily records of 2472 rain gauges in China at a resolution of $0.25^\circ \times 0.25^\circ$ from 1961 to 2014 (Wu and Gao 2013). The station data comprise 32 stations from 1961 to 2014 in the study area (Fig. 1). The GPCC data provide gridded gauge-analysis products derived from quality-controlled station data at a resolution $1^\circ \times 1^\circ$. The monthly CRU dataset is interpolated from more than 4000 weather stations over global land area with a resolution of $0.5^\circ \times 0.5^\circ$.

The daily and monthly reanalysis from the National Centers for Environmental Prediction and National Center for Atmospheric Research (NCEP–NCAR) with a horizontal resolution of $2.5^\circ \times 2.5^\circ$ from 1961 to 2014 (Kalnay et al. 1996) is used to analyze the water vapor transport and associated atmospheric circulations responsible for the cold season precipitation variability. The NCEP–NCAR reanalysis is considered sufficient enough to assess large-scale atmospheric features, since this dataset has been intensively employed in numerous studies for understanding atmospheric processes in Asia (e.g., Han et al. 2017; Huang et al. 2015). In this study, the daily and monthly zonal wind, meridional wind, omega (vertical velocity), geopotential height, specific humidity, and air temperature at 17 pressure levels are selected from NCEP–NCAR for the analysis.

A monthly SST dataset with a horizontal resolution of $1^\circ \times 1^\circ$ from 1961 to 2014 is extracted from the UK Met Office Hadley Centre data (Rayner et al. 2003) to investigate the role of the SST for the cold season precipitation variability. The Niño-3.4 index is defined as the areal mean SST of the region $5^\circ\text{N}–5^\circ\text{S}$, $120^\circ\text{–}170^\circ\text{W}$ in the tropical Pacific (Trenberth and Stepaniak 2001), which is provided by the NOAA/ESRL Physical Sciences Laboratory.

b. Methods

Different precipitation intensities over the TRH region were identified based on the daily precipitation amount distribution

(the criteria of classifications are shown in section 3b). The associated water vapor transport and atmospheric circulations corresponding to different precipitation intensities are investigated by composite analysis. In addition, anomalies of related atmospheric variables are calculated by removing the climatological mean from 1961 to 2014. Furthermore, to explore the response of the atmospheric circulation for the changed Walker circulation, the linear regression analysis with a method of least squares is used. This method is to regress one

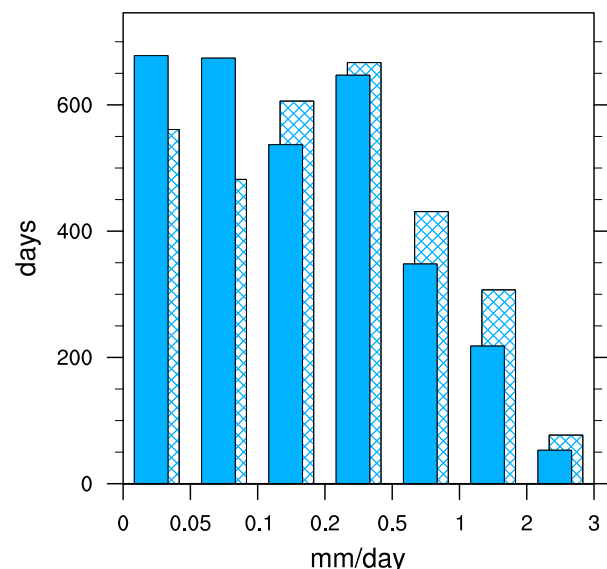


FIG. 3. Histogram of the cold season daily precipitation during the dry period (1961–75; 15 years) (front solid bars) and wet period (1995–2009; 15 years) (back hatched bars). The x axis gives the bins of the daily precipitation amount (mm day^{-1}) and the y axis gives the precipitation days (days) corresponding to different precipitation intensities.

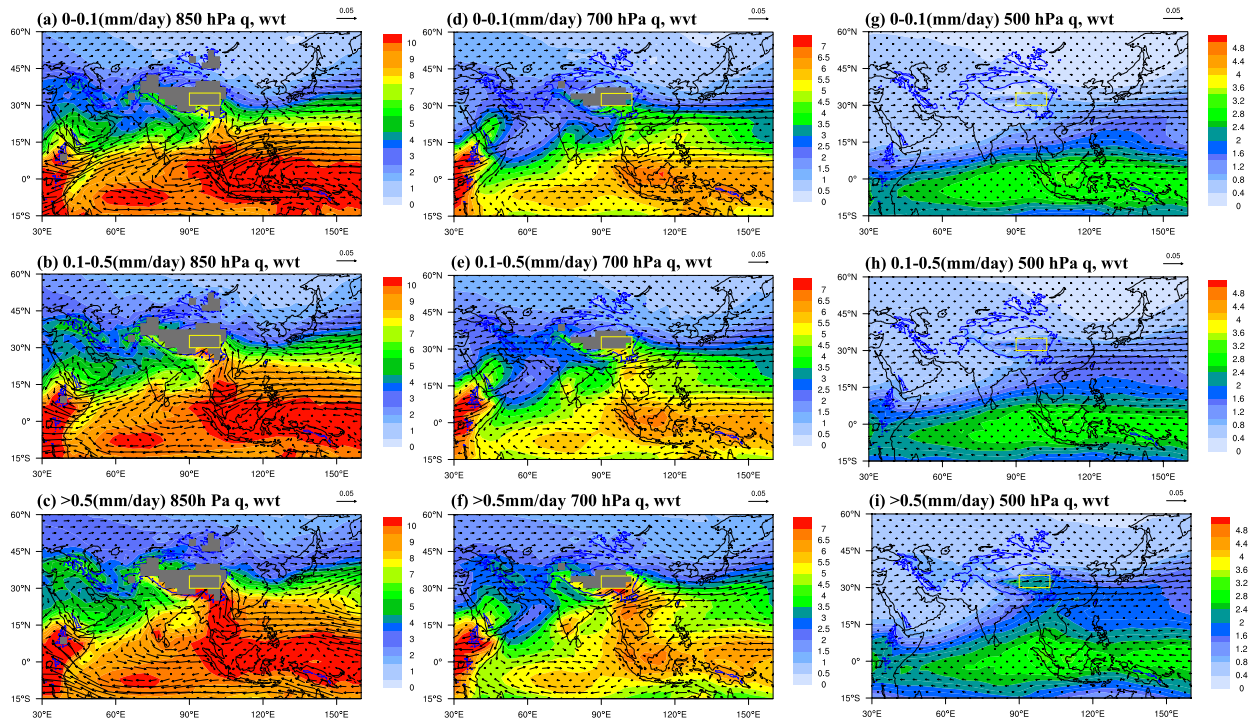


FIG. 4. Composite mean of water vapor transport (vectors; unit: $\text{kg m}^{-3} \text{s}^{-1}$) and specific humidity (colors; unit: g kg^{-1}) at (a)–(c) 850, (d)–(f) 700, and (g)–(i) 500 hPa corresponding to different categories of precipitation—(a),(d),(g) 0–0.1, (b),(e),(h) 0.1–0.5, and (c),(f),(i) $>0.5 \text{ mm day}^{-1}$ —for the total period of 1961–2014. Here q and wvt represent specific humidity and water vapor transport at a specific level, respectively. The curved blue lines delineate the 2000-m isohyposes.

space–time atmospheric variable y against one standardized domain-averaged variable of interest x for a certain period by employing the following linear regression model:

$$y = \alpha + \beta x, \quad (1)$$

where α and β denote the intercept and the slope (i.e., the regression coefficient) of the fitted regression line, respectively. The regression analysis is carried out at each grid cell in order to derive the spatial pattern of the regression coefficient β . Similar analyses can be found in numerous studies (Ao and Sun 2016; He et al. 2017; Huang et al. 2015; Wang et al. 2017). The Pearson's correlation coefficient is used to estimate the correlation between two continuous variables. The Student's t test is used to assess the statistical significance of correlation coefficients and the results of the atmospheric circulation analysis in this study.

3. Results and discussion

a. Spatiotemporal variations of the cold season precipitation

Figure 2a shows the CN05.1-derived temporal variation of the standardized cold season precipitation averaged over the TRH region from 1961 to 2014. The result displays a dry-to-wet transitional shift of the cold season precipitation in around the late 1980s. Within the investigated 54 years, largely negative anomalies are found during the period from 1961 to 1975 and

largely positive anomalies from 1995 to 2014. Figure 2b further shows the spatial pattern of trends in the cold season precipitation. Generally, significant positive trends are found over the entire study region. The positive trends from the northwest toward the southeast increase and reach the maximal values up to $10 \text{ mm decade}^{-1}$ in the southeastern TRH region. Averaged over the whole region, the cold season precipitation increases with a mean value of about $5.5 \text{ mm decade}^{-1}$. To examine the robustness of the result of the precipitation variation in the cold season, the station data in the study area, the GPCC and the CRU datasets are additionally used to show the variability of precipitation (see Fig. S1 in the online supplemental material). The Pearson correlation coefficients among the standardized time series of cold season precipitation derived from the four datasets are all above 0.85 and statistically significant at the 99% confidence level. Our result is also consistent with other studies that the cold season precipitation exhibits increasing trend from 1961 onward (Shi et al. 2016; Yi et al. 2013; Dong et al. 2020). The consistency between CN05.1 and the other datasets indicates that CN05.1 can reasonably represent the precipitation change over the TRH region (Shi et al. 2016; Zhou et al. 2016). Hence, the subsequent analyses about the associated atmospheric circulations of the precipitation variation are based on the daily CN05.1 data exclusively. To investigate the underlying mechanisms of the changed cold season precipitation, in the following, two subperiods—the wet period from 1995 to 2014 (with continuously positive

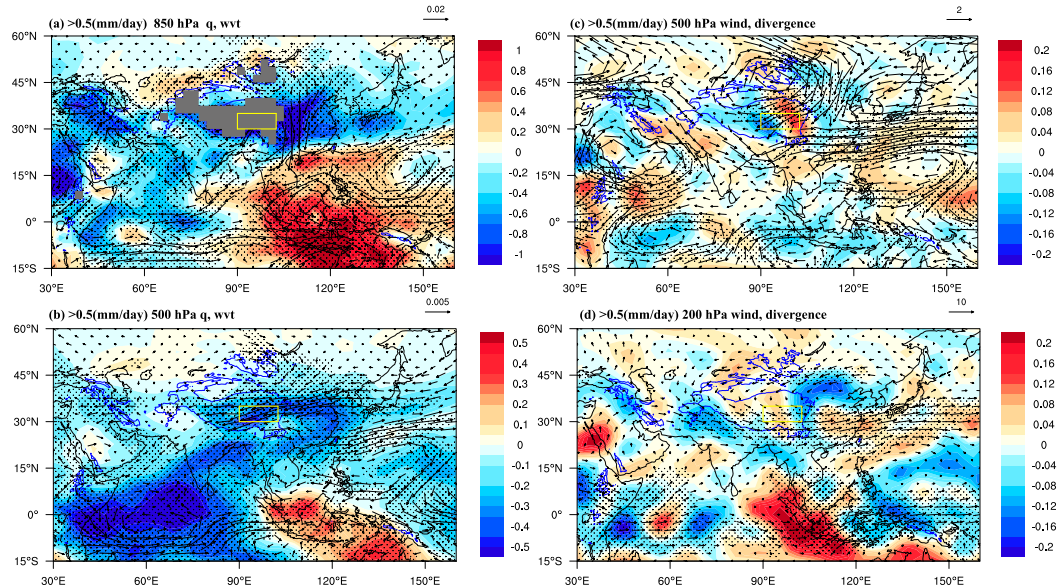


FIG. 5. (left) Difference of water vapor transport (vectors; unit: $\text{kg m}^{-1} \text{s}^{-1}$) and specific humidity (colors; unit: g kg^{-1}) at (a) 850 and (b) 500 hPa. (right) Differences of wind (vectors; unit: m s^{-1}) and its divergence (colors; 10^{-5}s^{-1}) at (c) 500 and (d) 200 hPa corresponding to moderate precipitation events between the wet period (1995–2009) and dry period (1961–75). The curved blue lines delineate the 2000-m isohypes. Superimposed dots indicate that the differences are statistically significant at the 95% confidence level; q and wvt represent specific humidity and water vapor transport at a specific level, respectively.

precipitation anomalies) and the dry period from 1961 to 1975 (with largely negative precipitation anomalies)—are selected for the analysis.

To evaluate whether the increased precipitation from the late 1980s is due to the increase of rainfall days or with intensified strength in single rainfall events, the histograms of daily precipitation from 1961 to 1975 and from 1995 to 2009 (15 years of the dry period and wet period separately) are further shown in Fig. 3. Figure 3 shows that moderate precipitation events ($>0.5 \text{ mm day}^{-1}$) increased by 220 days and days with no or virtually no precipitation ($<0.1 \text{ mm day}^{-1}$) decreased by 310 days during the wet period in comparison to the receptive days during the dry period. This indicates that the increased cold season precipitation during the wet period is mainly attributed to the increase of rainfall days and the moderate precipitation events.

b. Associated atmospheric circulations related to the cold season precipitation variability

To understand how the water vapor transport affects the intensity of cold-season precipitation in the study region, the precipitation amount shown in Fig. 3 is classified into three categories. No precipitation, light precipitation, and moderate precipitation events are defined as 0–0.1, 0.1–0.5, and $>0.5 \text{ mm day}^{-1}$, respectively. Composite means of water vapor transport and specific humidity at 850, 700, and 500 hPa corresponding to the classified three categories of precipitation from 1961 to 2014 are shown in Fig. 4. At 850 hPa (Figs. 4a–c), two water vapor transport pathways toward the TRH region are found: southwesterly water vapor transport along the southern edge of the TP conveying moisture

from the Arabian Sea and the Bay of Bengal (Simmonds et al. 1999) and southeasterly water vapor transport transporting moisture from the South China Sea and tropical oceans. A comparison of Figs. 4c and 4b indicates that the identified southwesterly and southeasterly moisture transport processes are both enhanced in case of enhanced cold season precipitation (i.e., from light precipitation to moderate precipitation). In association with the increased cold season precipitation intensity over the TRH region, there is a stronger anticyclone (around 30°N , 150°E) over the western North Pacific that expands westward (Figs. 4a–c). Indeed, the increased strength and westward expansion of the anticyclone over the western North Pacific can contribute to enhanced water vapor transport from the South China Sea and tropical oceans toward the TRH region. The southwesterly water vapor transport at the southern edge of the TP (at 700 hPa in Figs. 4d–f) and midlatitude westerly water vapor transport (at 500 hPa in Figs. 4g–i) are also more intense during enhanced cold season precipitation intensity.

Figure 3 reveals that moderate precipitation contributes the most to the increased cold season precipitation. Composite differences of water vapor transport and atmospheric circulations corresponding to moderate precipitation events during the wet period and the dry period are analyzed in Fig. 5. Figure 5a shows that the southwesterly water vapor transport at 850 hPa along the southern edge of the TP toward the TRH region decreases during the wet period. An anomalous anticyclone over the western North Pacific and an anomalous cyclone in Maritime Continent are observed, which enhance the equatorial easterly water vapor transport from the moister

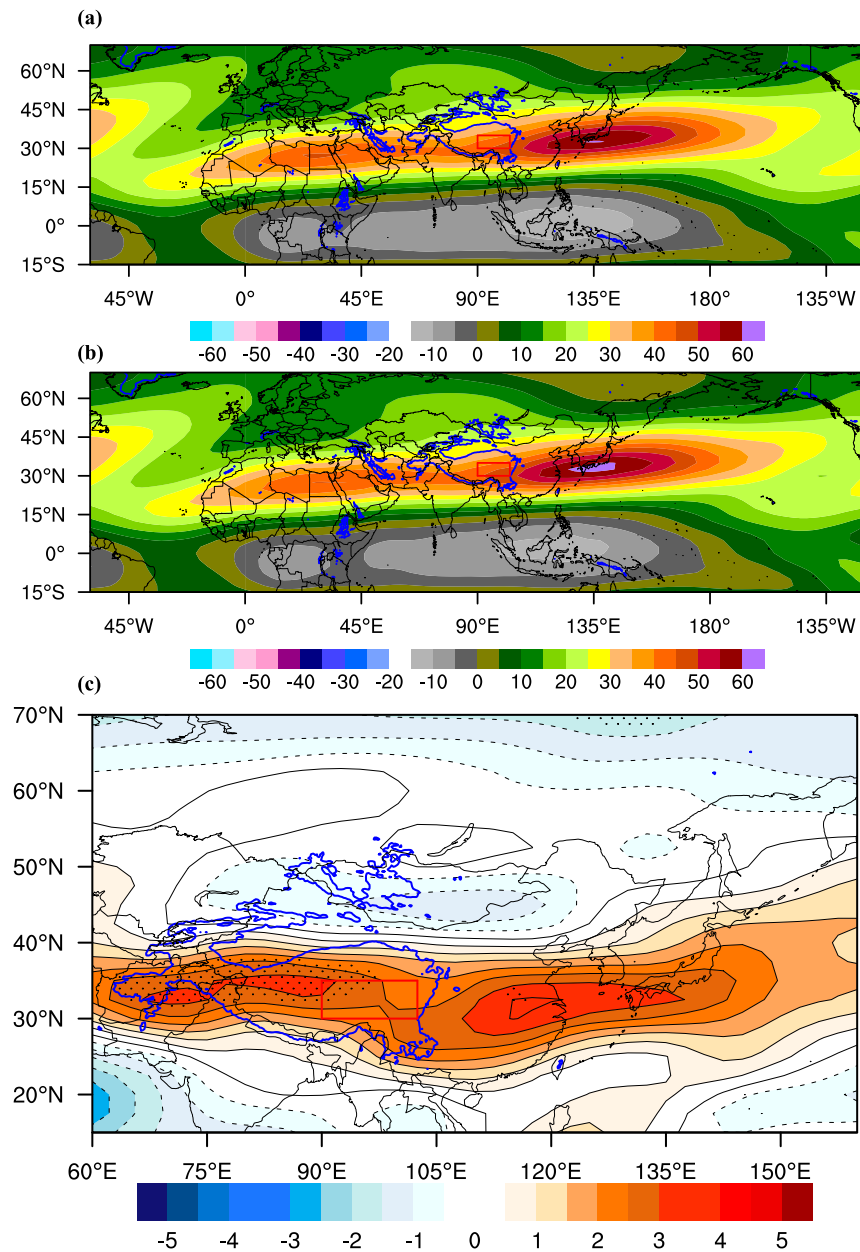


FIG. 6. Climatology of the cold season 200-hPa zonal wind (m s^{-1}) during the period of (a) 1961–75 and (b) 1995–2014 and (c) their differences. The curved blue lines delineate the 2000-m isohypes. Superimposed dots indicate that the anomalies are statistically significant at the 95% confidence level. The curved blue lines delineate the 2000-m isohypes.

tropical oceans and the South China Sea during the wet period. Besides, strong northerly water vapor transport anomalies appear over central China, which may suppress the eastward turning of southeasterly moisture transport and more water vapor is restrained in the south adjacent to the TRH region during the wet period (Fig. S2).

Figure 5b shows anomalous easterly water vapor transport and reduced specific humidity at 500 hPa in the study region during the wet period. Anomalous easterlies over the whole TP

and enhanced convergence over the west of the TRH region at 500 hPa are shown (Fig. 5c). It also should be noted that stronger anomalous easterlies are shown over the east of the TP, but smaller anomalous easterlies are shown over the west (Fig. 5c). The contrast of the wind anomalies over the east and west of the TP is favorable for the convergence over the inner TP (including the west of the TRH) and reduces the export of water vapor from the eastern boundary as addressed in other studies (Zhou et al. 2019; Lin et al. 2013; Sun et al. 2020).

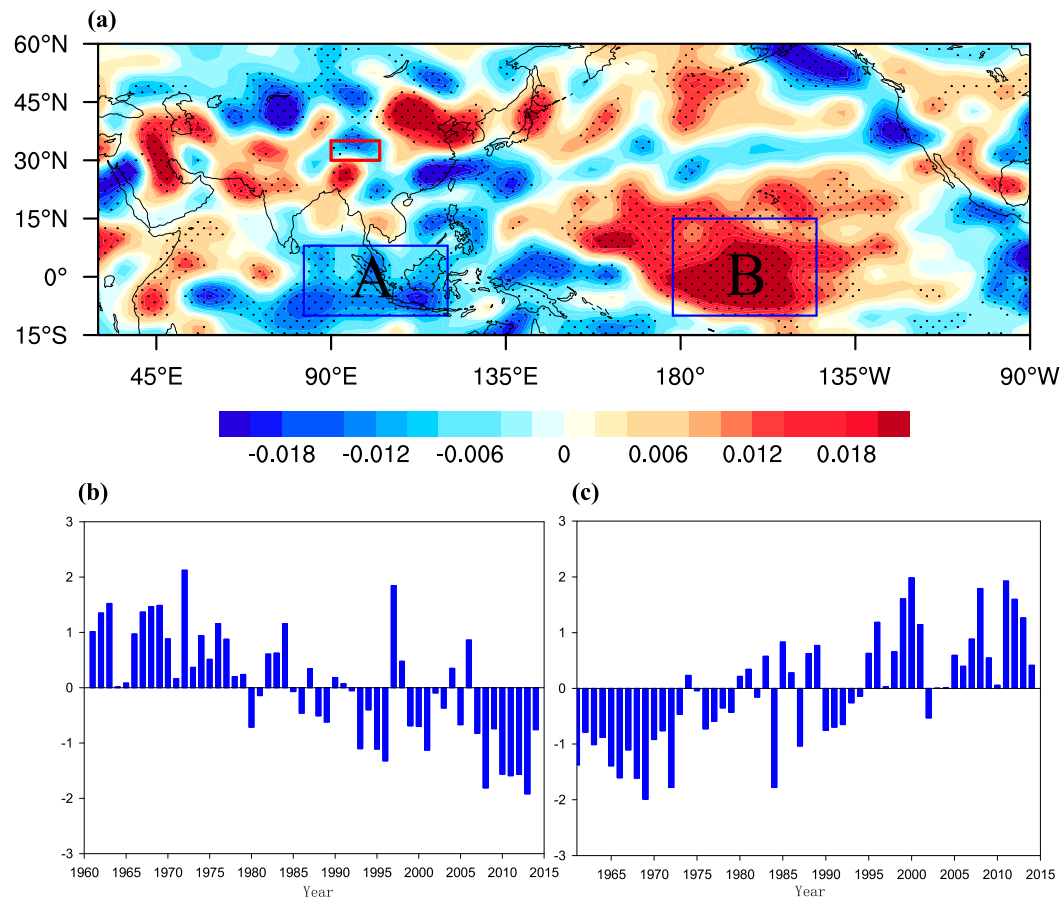


FIG. 7. (a) Differences of the cold season 500-hPa vertical velocity (Pa s^{-1}) between the periods 1995–2014 and 1961–75. Time series of the standardized cold season vertical velocity index (nondimensional), averaged over (b) area A and (c) area B from 1961 to 2014. Superimposed dots indicate that differences are statistically significant at the 95% confidence level.

This may be the reason why the stronger the easterly anomalies are at 500 hPa are, the more intense the cold season precipitation events are in the TRH region (Fig. 5c; see also Fig. S3). Also, the differences of 500-hPa winds between the wet period and the dry period show an anomalous anticyclone over the western North Pacific (Figs. 5c and 4c).

At 200 hPa, Fig. 5d shows enhanced westerlies and divergence above the study region. The enhanced westerlies and divergence at 200 hPa may be related to the change of East Asian subtropical westerly jet (EASJ). The EASJ is one of the most active circulation systems in the upper troposphere in central Asia and East Asia and has important influence on the variability of precipitation over East Asia (Yang et al. 2002). It is located in the southern edge of the TP in winter and the premonsoon season (Bao and You 2019; Huang et al. 2017). The TRH region is located in the entrance region of the jet stream and the weather and climate are considerably influenced by the variability of the subtropical jet during the cold season (Krishnamurti 1961). Figure 6 shows the climatology of the cold season 200-hPa zonal winds during the wet and dry periods and their corresponding difference. The jet core of the

EASJ for both periods is similarly located over southern Japan (Bao and You 2019; Huang et al. 2017), whereas the jet core during the wet period is strengthened and broadened than that during the dry period (Figs. 6a,b). The difference of the 200-hPa zonal winds between the wet period and the dry period (Fig. 6c) shows a strengthened wind around $30^{\circ}\text{--}40^{\circ}\text{N}$. As a result, a pronounced acceleration of 200-hPa zonal wind in the study region appears during the wet period. On the one hand, the strengthened EASJ contributes to the divergence at upper levels (Fig. 5d). On the other hand, the strengthened EASJ may be conducive to the anomalous ascending motion above the TRH region (Fig. 7) due to a secondary circulation over the entrance of the jet stream (Bao and You 2019), which is beneficial to the increased precipitation.

c. Teleconnections between the enhanced Walker circulation and the increased cold season precipitation

The difference of vertical velocity at 500 hPa in the cold season between the wet and the dry period not only shows anomalous ascending motion (negative anomalies) in the study region but also anomalous ascending motion over the tropical

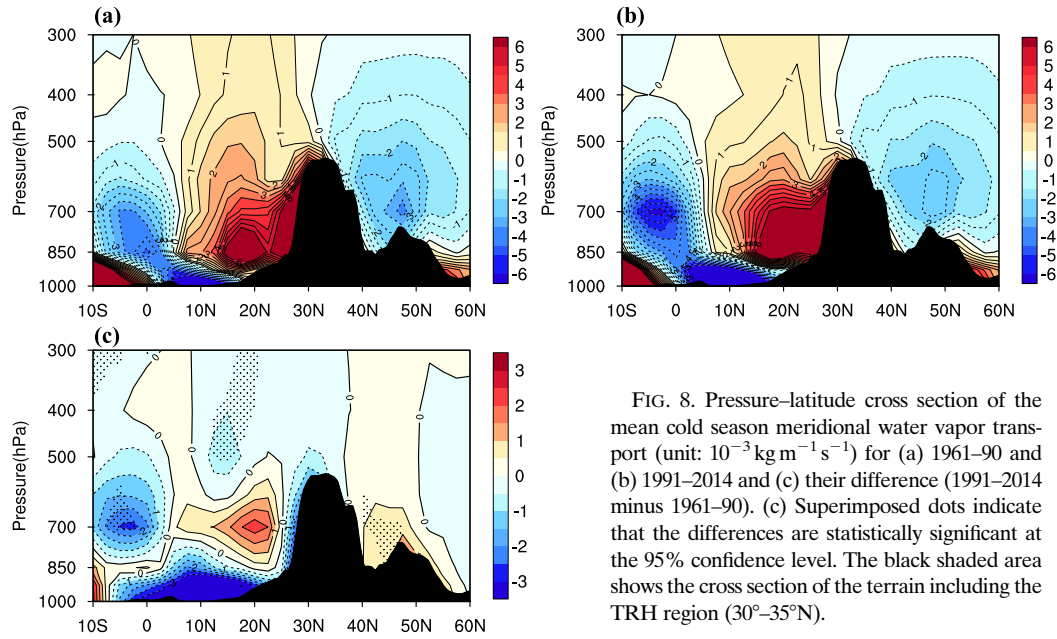


FIG. 8. Pressure–latitude cross section of the mean cold season meridional water vapor transport (unit: $10^{-3} \text{ kg m}^{-1} \text{ s}^{-1}$) for (a) 1961–90 and (b) 1991–2014 and (c) their difference (1991–2014 minus 1961–90). (c) Superimposed dots indicate that the differences are statistically significant at the 95% confidence level. The black shaded area shows the cross section of the terrain including the TRH region (30° – 35° N).

Indo–western Pacific (referred to as area A) and anomalous descending motion over the equatorial central–eastern Pacific (referred to as area B), respectively (Fig. 7a). The result of the changed vertical motions over the tropical ocean implies an enhanced Walker circulation during the wet period (Bjerknes 1969; Ma and Zhou 2016; Sohn et al. 2013; England et al. 2014; McGregor et al. 2014). Previous studies have demonstrated that the anomalous ascending motions over the tropical oceans can enhance convective activities at local scales, which have impacts on midlatitude atmospheric circulations via teleconnections and thereby influence precipitation regimes (Zhang and Webster

1989; Lau and Lim 1984). It is found that the temporal variations of the standardized vertical velocity averaged over area A and area B from 1961 to 2014 shows transitional shifts around the late 1980s, which is consistent with the time of the identified shift of the cold season precipitation in the study area (shown in section 3a) (Figs. 7b,c). To examine the relationship between the anomalous vertical motion over the tropical oceans and the cold season precipitation variation in the study region, we analyzed the correlations between the standardized cold season precipitation and the omega index over area A and area B. Results show that the variability of the cold season precipitation over the

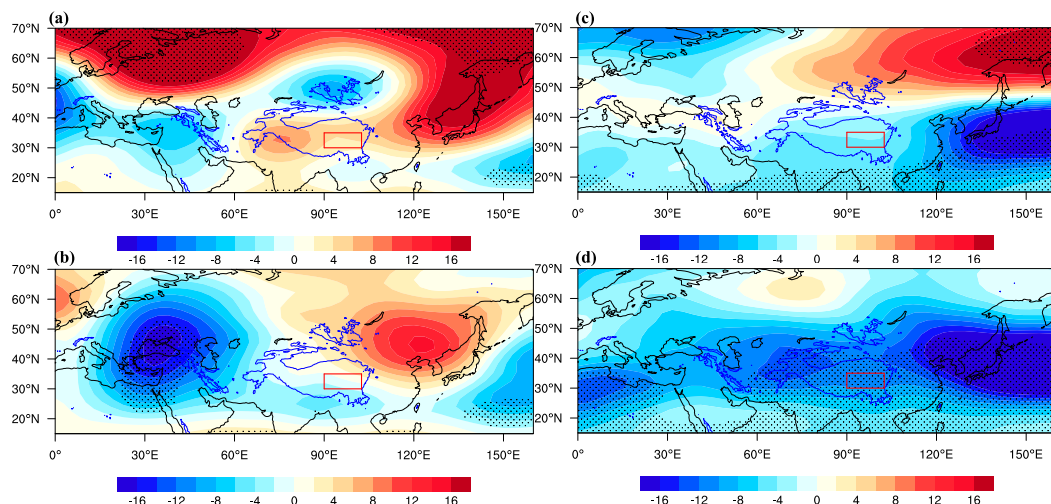


FIG. 9. Spatial pattern of the linear regression (gpm) of the cold season 500-hPa geopotential height against the standardized area A-averaged, cold season 500-hPa omega index during the period of (a) 1961–75 and (b) 1995–2014. (c),(d) As in (a) and (b), but for area B. Superimposed dots indicate that regression coefficients are statistically significant at the 95% confidence level. The curved blue lines delineate the 2000-m isohypes.

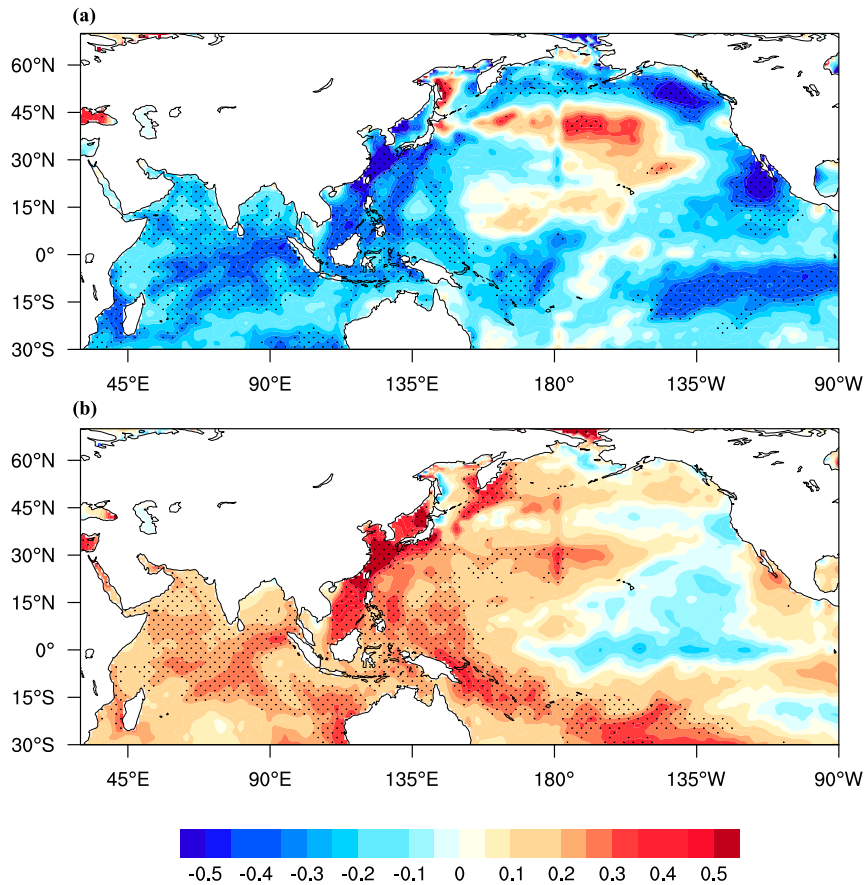


FIG. 10. Spatial pattern of the cold season SST anomalies ($^{\circ}\text{C}$) during (a) the dry period (1961–75) and (b) the wet period (1995–2014). The anomalies are derived based on the corresponding cold season climatology for the period of 1961–2014. Superimposed dots indicate that the anomalies are statistically significant at the 95% confidence level.

TRH region has a significant correlation with the anomalous vertical motion over the tropical oceans (area A: $R = -0.454$, $p < 0.01$; area B: $R = 0.662$, $p < 0.01$). Figure 8 further shows the cross section of meridional water vapor transport averaged from 90° to 102.5°E during 1961–90 and 1991–2014 and their corresponding difference. It reveals an enhancement of the southerly transport above 850 hPa due to the strengthening of the local Hadley circulation (HC) (Hartmann 2016) in the cold season (Fig. 8c). Thus, the changed Walker circulation is also accompanied by a change of local HC, which plays an important role in enhancing meridional water vapor transport from tropical oceans toward the TRH region (Hadley 1735; Webster 2004).

To further investigate how the enhanced Walker circulation affects the cold season precipitation variability in the study area via teleconnections, Fig. 9 depicts the regression patterns of the 500-hPa geopotential height against the omega index over area A and area B during the dry and wet periods. Figures 9a and 9b show the regression patterns of the cold season 500-hPa geopotential height against omega index over area A for dry and wet periods. During the dry period (Fig. 9a), a zonal pattern of the anomalous atmospheric circulation from upstream to downstream is found over 35° – 60°N

in Eurasia: positive anomalies of the 500-hPa geopotential height over around the Ural Mountains and the Okhotsk Sea, and negative anomalies over Mongolia. The negative anomalies of geopotential height over Mongolia should suppress the anomalous anticyclone to the north of the TRH region and thereby weaken the anomalous easterlies in the TP (Fig. 5c). Meanwhile, positive anomalies are found in the study region, which suppresses the ascending motion and convergence there during the dry period. In contrast, during the wet period (Fig. 9b), the negative anomalies to the north of the TRH region disappeared, while the study area is dominated by negative geopotential height anomalies. In addition, the TRH region is located ahead of the trough in Europe and behind the ridge in northeastern China, which should cause enhanced ascending motion above the TRH region (Figs. 5c and 8a) (Holton and Staley 1973). Figures 9c and 9d show the regression patterns of the cold season geopotential height at 500 hPa against the omega index over area B during the dry and wet periods. It is shown that a meridional dipole pattern exists over the North Pacific (significantly negative anomalies) and the midlatitude region around the Aleutian Islands (significantly positive anomalies), which is characterized as a negative phase of the North Pacific

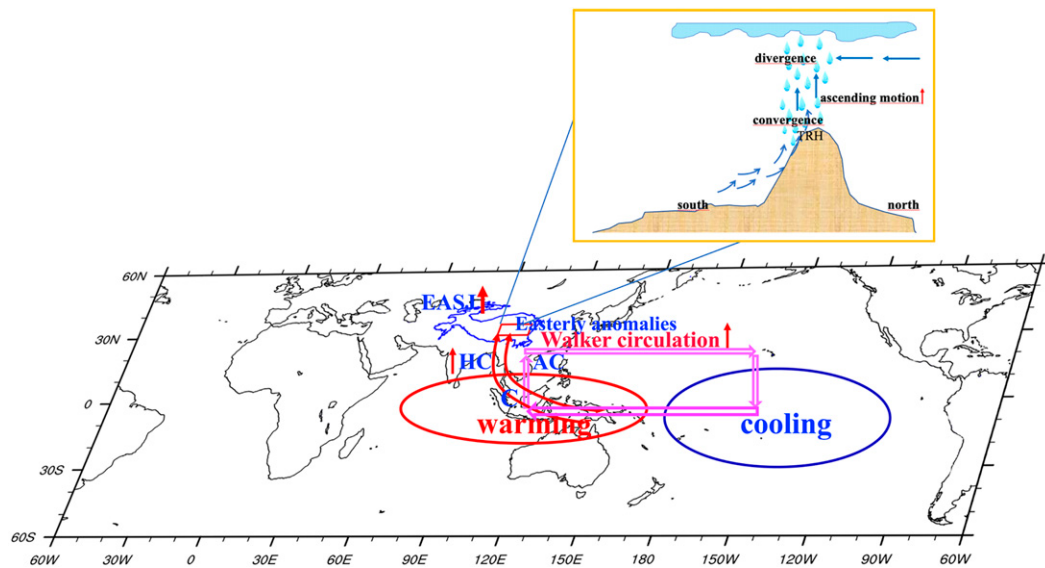


FIG. 11. Schematic diagram of the associated atmospheric mechanisms of the increased cold season precipitation over the TRH region from the late 1980s. The curved blue lines delineate the 2000-m isohyps. AC = anomalous anticyclone, C = anomalous cyclone, HC = Hadley circulation. The red up arrows indicate enhancement of the EASJ, the Walker circulation, the Hadley circulation, and ascending motion.

Oscillation (NPO) pattern (Rogers 1981) during the dry period. Such a negative NPO pattern found during the dry period can suppress westward expansions of the anticyclone over the western North Pacific (Han et al. 2020) (Fig. 4), and thus weaken the water vapor transport from the South China Sea and tropical oceans (Figs. 4 and 5). In contrast, during the wet period the positive anomalies of geopotential height over the Aleutian Islands disappeared and the negative anomalies in the western North Pacific enhanced and exhibited westward expansion.

d. Possible causes for the increased cold season precipitation

The anomalies of the SST in the cold season during the dry and wet periods are further examined as SST is a key factor affecting atmospheric circulation. Figure 10a shows significant negative SST anomalies over the tropical Indo–western Pacific (El Niño-like SST pattern) during the dry period. Corresponding to the wet period, significant positive SST anomalies over the tropical Indo–western Pacific and negative anomalies over the equatorial central-eastern Pacific (a La Niña-like SST pattern) are observed (Fig. 10b). The cooling equatorial central-eastern Pacific may cause the stronger anomalous anticyclone in the western North Pacific, while the abnormal heating over the tropical Indo–western Pacific results in the higher air temperature and specific humidity here, and induces the anomalous cyclone in Maritime Continent (Fig. 5a; see also Fig. S2). The anomalous cyclone in Maritime Continent and the stronger anticyclone over the western North Pacific leads to enhanced water vapor transport from the tropical oceans and the South China Sea (Figs. 5 and 6).

The regression pattern of the 500-hPa vertical velocity against the sign-inversed standardized Niño-3.4 index indicates

that the convective ascending motion over the tropical western Pacific is strengthened significantly during the wet period (Ma and Zhou 2016; Sohn et al. 2013) (Fig. S4). Thus, the Walker circulation is enhanced by the La Niña-like SST pattern. The changed Walker circulation encourages the anomalous mid-latitude atmospheric circulations, which is conducive to the easterly anomalies in the study area and the westward expansion of the anticyclone in the western North Pacific (Wu et al. 2020) (Figs. 5a,c). Meanwhile, the changed Walker circulation is accompanied by a strengthened local HC (Nguyen et al. 2013; Guo and Tan 2018), which leads to the enhanced meridional water vapor fluxes toward the TP. Furthermore, the enhanced easterly anomalies in the TP and the strengthened EASJ cause enhanced convergence and anomalous ascending motion above the TRH region, and enhanced divergence at upper levels. The abovementioned conditions jointly cause more precipitation in the cold season over the TRH region from the late 1980s. Finally, the role of SST and associated atmospheric mechanisms for the increased cold season precipitation over the TRH region is summarized in Fig. 11.

4. Summary and conclusions

In this study, the spatiotemporal variations of the cold season (October to April) precipitation over the TRH region during the period of 1961–2014 have been investigated based on the high-resolution daily China gridded precipitation dataset CN05.1. The results show an increasing trend of the cold season precipitation from 1961 to 2014 and with a dry-to-wet shift in around the late 1980s. Using the daily and monthly reanalysis of NCEP–NCAR, underlying atmospheric mechanisms for the change of the cold season precipitation are explored by comparing the related atmospheric circulations

during a dry period (1961–75) and a wet period (1995–2014). Our results show that the cold season precipitation variability over the TRH region is associated with the southwesterly and southeasterly water vapor transport at low level (850 hPa) and midlatitude westerly water vapor transport at middle level (500 hPa). The increased precipitation is possibly related to the anomalous cyclone in the Maritime Continent and anomalous anticyclone in the western North Pacific, which lead to the enhanced water vapor transport from the South China Sea and tropical oceans. The stronger easterly anomalies over the east of the TP can be favorable for the convergence above the study area and reduce the export of water vapor from the eastern boundary. In addition, the strengthened EASJ possibly leads to enhanced divergence at upper levels (200 hPa) and anomalous ascending motion above the TRH region.

We further found that the SST may be a key factor influencing the change of the cold season precipitation over the TRH region. The abnormal warming of the tropical Indo-western Pacific causes strengthened HC, which plays a vital role in the meridional moisture transport toward the study area. The SST gradients between the tropical Indo-western Pacific and the equatorial central-eastern Pacific drive the enhanced Walker circulation from the late 1980s, which possibly encourages the anomalous midlatitude atmospheric circulations via teleconnections. Corresponding to the anomalous vertical motions over tropical oceans during the dry period, a zonal teleconnection pattern of anomalous atmospheric circulations from upstream to downstream around 35°–60°N in Eurasia depicts positive anomalies of the 500-hPa geopotential height in around the Ural Mountains and the Okhotsk Sea, and negative anomalies in Mongolia, which should suppress the easterly anomalies over the TP. In addition, a negative phase of NPO pattern is found, which can suppress the westward expansions of the anticyclone in the western North Pacific. During the wet period, the TRH region is dominated by negative anomalies of geopotential height and negative anomalies in Mongolia are observed, while the negative phase of the NPO pattern disappeared.

Our results are based on one reanalysis (i.e., NCEP–NCAR) because of the long timespan (Wu et al. 2005). In the future, an ensemble analysis with multiple data sources (Li et al. 2018) could be applied in other cases to narrow down uncertainties in the choice of reanalysis. Moreover, it should be acknowledged that our large-scale atmospheric circulation analysis is only able to explore the possible linkage and relations of the atmosphere associated with the increased cold season precipitation. The land surface also can significantly affect the atmospheric branch of the hydrological cycle (Seneviratne et al. 2010, 2006). Regional climate models are a tool that has been extensively used to explore land-atmosphere interactions (Wei et al. 2015; Zhang et al. 2019; Arnault et al. 2016). High spatial and temporal resolution modeling at regional scales is needed to depict the role of land-atmosphere interactions for the cold season precipitation change over the TRH region in the future.

Acknowledgments. This research was supported by the National Key Research and Development Program of China

(2018YFC0406602) and Chinese Scholarship Council. Jianhui Wei and Joël Arnault are financially supported by the German Research Foundation grants (DFG, AccHydro KU 2090/11-1 and AR 1183/2-1). Zhenyu Zhang is supported by the German Federal Ministry of Science and Education (BMBF) project (SALDi, 01LL1701B), and Kun Zhang is supported by the National Natural Science Foundation of China (41901381). We thank the editor and three anonymous reviewers for their helpful comments.

Data availability statement. The CN05.1 data are obtained from the China Meteorology Administration's National Climate Center. The NCEP–NCAR reanalysis is downloaded from <https://psl.noaa.gov/data/gridded/data.ncep.reanalysis.html>. The HadISST dataset is downloaded from <https://www.metoffice.gov.uk/hadobs/hadisst/>. The GPCC precipitation dataset is downloaded from https://psl.noaa.gov/data/gridded/data_gpcc.html. The CRU precipitation dataset is downloaded from <https://crudata.uea.ac.uk/cru/data/hrg/>. The monthly Niño-3.4 index is downloaded from https://psl.noaa.gov/gcos_wgsp/Timeseries/Nino34/.

REFERENCES

- Ao, J., and J. Sun, 2016: Decadal change in factors affecting winter precipitation over eastern China. *Climate Dyn.*, **46**, 111–121, <https://doi.org/10.1007/s00382-015-2572-7>.
- Arnault, J., R. Knoche, J. Wei, and H. Kunstmann, 2016: Evaporation tagging and atmospheric water budget analysis with WRF: A regional precipitation recycling study for West Africa. *Water Resour. Res.*, **52**, 1544–1567, <https://doi.org/10.1002/2015WR017704>.
- Bai, W., X. Chen, Y. Tang, Y. He, and Y. Zheng, 2019: Temporal and spatial changes of soil moisture and its response to temperature and precipitation over the Tibetan Plateau. *Hydrol. Sci. J.*, **64**, 1370–1384, <https://doi.org/10.1080/02626667.2019.1632459>.
- Bao, Y., and Q. You, 2019: How do westerly jet streams regulate the winter snow depth over the Tibetan Plateau? *Climate Dyn.*, **53**, 353–370, <https://doi.org/10.1007/s00382-018-4589-1>.
- Beniston, M., 2003: Climatic change in mountain regions: A review of possible impacts. *Climatic Change*, **59**, 5–31, <https://doi.org/10.1023/A:1024458411589>.
- Bjerknes, J., 1969: Atmospheric teleconnections from the equatorial Pacific. *Mon. Wea. Rev.*, **97**, 163–172, [https://doi.org/10.1175/1520-0493\(1969\)097<0163:ATFTEP>2.3.CO;2](https://doi.org/10.1175/1520-0493(1969)097<0163:ATFTEP>2.3.CO;2).
- Boos, W. R., and Z. Kuang, 2010: Dominant control of the South Asian monsoon by orographic insulation versus plateau heating. *Nature*, **463**, 218–222, <https://doi.org/10.1038/nature08707>.
- Chen, B., X. Zhang, J. Tao, J. Wu, J. Wang, P. Shi, Y. Zhang, and C. Yu, 2014: The impact of climate change and anthropogenic activities on alpine grassland over the Qinghai-Tibet Plateau. *Agric. For. Meteor.*, **189–190**, 11–18, <https://doi.org/10.1016/j.agrformet.2014.01.002>.
- Chen, F., and R. Avissar, 1994: Impact of land-surface moisture variability on local shallow convective cumulus and precipitation in large-scale models. *J. Appl. Meteor.*, **33**, 1382–1401, [https://doi.org/10.1175/1520-0450\(1994\)033<1382:IOLSMV>2.0.CO;2](https://doi.org/10.1175/1520-0450(1994)033<1382:IOLSMV>2.0.CO;2).
- Cuo, L., Y. Zhang, Q. Wang, L. Zhang, B. Zhou, Z. Hao, and F. Su, 2013: Climate change on the northern Tibetan Plateau during 1957–2009: Spatial patterns and possible mechanisms. *J. Climate*, **26**, 85–109, <https://doi.org/10.1175/JCLI-D-11-00738.1>.

- de Oliveira, V. A., C. R. de Mello, M. R. Viola, and R. Srinivasan, 2017: Assessment of climate change impacts on streamflow and hydropower potential in the headwater region of the Grande river basin, southeastern Brazil. *Int. J. Climatol.*, **37**, 5005–5023, <https://doi.org/10.1002/joc.5138>.
- Dong, Y., J. Zhai, Y. Zhao, H. Li, Q. Wang, S. Jiang, H. Chang, and Z. Ding, 2020: Teleconnection patterns of precipitation in the Three-River Headwaters region, China. *Environ. Res. Lett.*, **15**, 104050, <https://doi.org/10.1088/1748-9326/aba8c0>.
- England, M. H., and Coauthors, 2014: Recent intensification of wind-driven circulation in the Pacific and the ongoing warming hiatus. *Nat. Climate Change*, **4**, 222–227, <https://doi.org/10.1038/nclimate2106>.
- Fu, G., Z. X. Shen, and X. Z. Zhang, 2018: Increased precipitation has stronger effects on plant production of an alpine meadow than does experimental warming in the northern Tibetan Plateau. *Agric. For. Meteor.*, **249**, 11–21, <https://doi.org/10.1016/j.agrmet.2017.11.017>.
- Gao, Y., H. Wang, and S. Li, 2013: Influences of the Atlantic Ocean on the summer precipitation of the southeastern Tibetan Plateau. *J. Geophys. Res.*, **118**, 3534–3544, <https://doi.org/10.1002/jgrd.50290>.
- Guo, Y., and C. Wang, 2014: Trends in precipitation recycling over the Qinghai-Xizang Plateau in last decades. *J. Hydrol.*, **517**, 826–835, <https://doi.org/10.1016/j.jhydrol.2014.06.006>.
- , and Z. M. Tan, 2018: The Hadley circulation regime change: Combined effect of the western Pacific warming and increased ENSO amplitude. *J. Climate*, **31**, 9739–9751, <https://doi.org/10.1175/JCLI-D-18-0306.1>.
- Gustafsson, M., D. Rayner, and D. Chen, 2010: Extreme rainfall events in southern Sweden: Where does the moisture come from? *Tellus*, **62A**, 605–616, <https://doi.org/10.1111/j.1600-0870.2010.00456.x>.
- Hadley, G., 1735: VI. Concerning the cause of the general trade-winds. *Philos. Trans. Roy. Soc. London*, **39**, 58–62, <https://doi.org/10.1098/rstl.1735.0014>.
- Han, T., H. Wang, and J. Sun, 2017: Strengthened relationship between eastern ENSO and summer precipitation over northeastern China. *J. Climate*, **30**, 4497–4512, <https://doi.org/10.1175/JCLI-D-16-0551.1>.
- , M. Zhang, B. Zhou, X. Hao, and S. Li, 2020: Strengthened relationship between tropical west Pacific and midsummer precipitation over northeast China after the mid-1990s. *J. Climate*, **33**, 6833–6848, <https://doi.org/10.1175/JCLI-D-19-0957.1>.
- Harris, I., P. D. Jones, T. J. Osborn, and D. H. Lister, 2014: Updated high-resolution grids of monthly climatic observations—The CRU TS3.10 dataset. *Int. J. Climatol.*, **34**, 623–642, <https://doi.org/10.1002/joc.3711>.
- Hartmann, D. L., 2016: *Global Physical Climatology*. Elsevier, 498 pp.
- He, S., Y. Gao, F. Li, H. Wang, and Y. He, 2017: Impact of Arctic Oscillation on the East Asian climate: A review. *Earth-Sci. Rev.*, **164**, 48–62, <https://doi.org/10.1016/j.earscirev.2016.10.014>.
- Holton, J. R., and D. O. Staley, 1973: An introduction to dynamic meteorology. *Amer. J. Phys.*, **41**, 752–754, <https://doi.org/10.1119/1.1987371>.
- Hu, J., and A. Duan, 2015: Relative contributions of the Tibetan Plateau thermal forcing and the Indian Ocean Sea surface temperature basin mode to the interannual variability of the East Asian summer monsoon. *Climate Dyn.*, **45**, 2697–2711, <https://doi.org/10.1007/s00382-015-2503-7>.
- Huang, D., A. Dai, J. Zhu, Y. Zhang, and X. Kuang, 2017: Recent winter precipitation changes over eastern China in different warming periods and the associated East Asian jets and oceanic conditions. *J. Climate*, **30**, 4443–4462, <https://doi.org/10.1175/JCLI-D-16-0517.1>.
- Huang, W., S. Feng, J. Chen, and F. Chen, 2015: Physical mechanisms of summer precipitation variations in the Tarim Basin in northwestern China. *J. Climate*, **28**, 3579–3591, <https://doi.org/10.1175/JCLI-D-14-00395.1>.
- Jiang, C., and L. Zhang, 2016: Ecosystem change assessment in the Three-River Headwater region, China: Patterns, causes, and implications. *Ecol. Eng.*, **93**, 24–36, <https://doi.org/10.1016/j.ecoleng.2016.05.011>.
- , D. Li, Y. Gao, W. Liu, and L. Zhang, 2017: Impact of climate variability and anthropogenic activity on streamflow in the Three Rivers Headwater Region, Tibetan Plateau, China. *Theor. Appl. Climatol.*, **129**, 667–681, <https://doi.org/10.1007/s00704-016-1833-7>.
- Kalnay, E., and Coauthors, 1996: The NCEP/NCAR 40-Year Reanalysis Project. *Bull. Amer. Meteor. Soc.*, **77**, 437–471, [https://doi.org/10.1175/1520-0477\(1996\)077<0437:TNYRP>2.0.CO;2](https://doi.org/10.1175/1520-0477(1996)077<0437:TNYRP>2.0.CO;2).
- Kang, S., Y. Xu, Q. You, W. A. Flügel, N. Pepin, and T. Yao, 2010: Review of climate and cryospheric change in the Tibetan Plateau. *Environ. Res. Lett.*, **5**, 015101, <https://doi.org/10.1088/1748-9326/5/1/015101>.
- Krishnamurti, T. N., 1961: The subtropical jet stream of winter. *J. Meteor.*, **18**, 172–191, [https://doi.org/10.1175/1520-0469\(1961\)018<0172:TSJSOW>2.0.CO;2](https://doi.org/10.1175/1520-0469(1961)018<0172:TSJSOW>2.0.CO;2).
- Lau, K. M., and H. Lim, 1984: On the dynamics of equatorial forcing of climate teleconnections. *J. Atmos. Sci.*, **41**, 161–176, [https://doi.org/10.1175/1520-0469\(1984\)041<0161:OTDOEF>2.0.CO;2](https://doi.org/10.1175/1520-0469(1984)041<0161:OTDOEF>2.0.CO;2).
- Li, F., Y. Zhang, Z. Xu, J. Teng, C. Liu, W. Liu, and F. Mpelasoka, 2013: The impact of climate change on runoff in the southeastern Tibetan Plateau. *J. Hydrol.*, **505**, 188–201, <https://doi.org/10.1016/j.jhydrol.2013.09.052>.
- Li, P., T. Zhou, and X. Chen, 2018: Water vapor transport for spring persistent rains over southeastern China based on five reanalysis datasets. *Climate Dyn.*, **51**, 4243–4257, <https://doi.org/10.1007/s00382-017-3680-3>.
- Li, X., G. Brierley, D. Shi, Y. Xie, and H. Sun, 2012: Ecological protection and restoration in Sanjiangyuan National Nature Reserve, Qinghai Province, China. *Perspectives on Environmental Management and Technology in Asian River Basins*, D. Higgitt, Ed., Springer, 93–120.
- Liang, L., L. Li, C. Liu, and L. Cuo, 2013: Climate change in the Tibetan Plateau Three Rivers Source Region: 1960–2009. *Int. J. Climatol.*, **33**, 2900–2916, <https://doi.org/10.1002/joc.3642>.
- Lin, C., K. Yang, J. Qin, and R. Fu, 2013: Observed coherent trends of surface and upper-air wind speed over China since 1960. *J. Climate*, **26**, 2891–2903, <https://doi.org/10.1175/JCLI-D-12-00093.1>.
- Liu, T., P. Willems, X. L. Pan, A. M. Bao, X. Chen, F. Veroustraete, and Q. H. Dong, 2011: Climate change impact on water resource extremes in a headwater region of the Tarim Basin in China. *Hydrol. Earth Syst. Sci.*, **15**, 3511–3527, <https://doi.org/10.5194/hess-15-3511-2011>.
- Liu, X., and B. Chen, 2000: Climatic warming in the Tibetan Plateau during recent decades. *Int. J. Climatol.*, **20**, 1729–1742, [https://doi.org/10.1002/1097-0088\(20001130\)20:14<1729::AID-JOC556>3.0.CO;2-Y](https://doi.org/10.1002/1097-0088(20001130)20:14<1729::AID-JOC556>3.0.CO;2-Y).
- , and Z.-Y. Yin, 2001: Spatial and temporal variation of summer precipitation over the eastern Tibetan Plateau and the North Atlantic Oscillation. *J. Climate*, **14**, 2896–2909, [https://doi.org/10.1175/1520-0442\(2001\)014<2896:SATVOS>2.0.CO;2](https://doi.org/10.1175/1520-0442(2001)014<2896:SATVOS>2.0.CO;2).
- , Z. Cheng, L. Yan, and Z.-Y. Yin, 2009: Elevation dependency of recent and future minimum surface air temperature trends in the

- Tibetan Plateau and its surroundings. *Global Planet. Change*, **68**, 164–174, <https://doi.org/10.1016/j.gloplacha.2009.03.017>.
- , J. Zhang, X. Zhu, Y. Pan, Y. Liu, D. Zhang, and Z. Lin, 2014: Spatiotemporal changes in vegetation coverage and its driving factors in the Three-River Headwaters Region during 2000–2011. *J. Geogr. Sci.*, **24**, 288–302, <https://doi.org/10.1007/s11442-014-1088-0>.
- Ma, S., and T. Zhou, 2016: Robust strengthening and westward shift of the tropical Pacific Walker circulation during 1979–2012: A comparison of 7 sets of reanalysis data and 26 CMIP5 models. *J. Climate*, **29**, 3097–3118, <https://doi.org/10.1175/JCLI-D-15-0398.1>.
- Ma, Y., M. Lu, H. Chen, M. Pan, and Y. Hong, 2018: Atmospheric moisture transport versus precipitation across the Tibetan Plateau: A mini-review and current challenges. *Atmos. Res.*, **209**, 50–58, <https://doi.org/10.1016/j.atmosres.2018.03.015>.
- McGregor, S., A. Timmermann, M. F. Stuecker, M. H. England, M. Merrifield, F. F. Jin, and Y. Chikamoto, 2014: Recent walker circulation strengthening and Pacific cooling amplified by Atlantic warming. *Nat. Climate Change*, **4**, 888–892, <https://doi.org/10.1038/nclimate2330>.
- Nguyen, H., A. Evans, C. Lucas, I. Smith, and B. Timbal, 2013: The Hadley circulation in reanalyses: Climatology, variability, and change. *J. Climate*, **26**, 3357–3376, <https://doi.org/10.1175/JCLI-D-12-00224.1>.
- Nijssen, B., G. M. O'Donnell, A. F. Hamlet, and D. P. Lettenmaier, 2001: Hydrologic sensitivity of global rivers to climate change. *Climatic Change*, **50**, 143–175, <https://doi.org/10.1023/A:1010616428763>.
- Pepin, N. C., and J. D. Lundquist, 2008: Temperature trends at high elevations: Patterns across the globe. *Geophys. Res. Lett.*, **35**, L14701, <https://doi.org/10.1029/2008GL034026>.
- , —, and Coauthors, 2015: Elevation-dependent warming in mountain regions of the world. *Nat. Climate Change*, **5**, 424–430, <https://doi.org/10.1038/nclimate2563>.
- Qin, J., K. Yang, S. Liang, and X. Guo, 2009: The altitudinal dependence of recent rapid warming over the Tibetan Plateau. *Climatic Change*, **97**, 321–327, <https://doi.org/10.1007/s10584-009-9733-9>.
- Rangwala, I., and J. R. Miller, 2012: Climate change in mountains: A review of elevation-dependent warming and its possible causes. *Climatic Change*, **114**, 527–547, <https://doi.org/10.1007/s10584-012-0419-3>.
- , —, and M. Xu, 2009: Warming in the Tibetan Plateau: Possible influences of the changes in surface water vapor. *Geophys. Res. Lett.*, **36**, L06703, <https://doi.org/10.1029/2009GL037245>.
- Rayner, N. A., D. E. Parker, E. B. Horton, C. K. Folland, L. V. Alexander, D. P. Rowell, E. C. Kent, and A. Kaplan, 2003: Global analyses of sea surface temperature, sea ice, and night marine air temperature since the late nineteenth century. *J. Geophys. Res.*, **108**, 4407, <https://doi.org/10.1029/2002JD002670>.
- Rogers, J. C., 1981: The North Pacific Oscillation. *J. Climatol.*, **1**, 39–57, <https://doi.org/10.1002/joc.3370010106>.
- Schneider, U., M. Ziese, A. Meyer-Christoffer, P. Finger, E. Rustemeier, and A. Becker, 2016: The new portfolio of global precipitation data products of the Global Precipitation Climatology Centre suitable to assess and quantify the global water cycle and resources. *Proc. IAHS*, **374**, 29–34, <https://doi.org/10.5194/piahs-374-29-2016>.
- Seneviratne, S. I., D. Lüthi, M. Litschi, and C. Schär, 2006: Land–atmosphere coupling and climate change in Europe. *Nature*, **443**, 205–209, <https://doi.org/10.1038/nature05095>.
- , T. Corti, E. L. Davin, M. Hirschi, E. B. Jaeger, I. Lehner, B. Orłowsky, and A. J. Teuling, 2010: Investigating soil moisture–climate interactions in a changing climate: A review. *Earth-Sci. Rev.*, **99**, 125–161, <https://doi.org/10.1016/j.earscirev.2010.02.004>.
- Shaman, J., and E. Tziperman, 2005: The effect of ENSO on Tibetan Plateau snow depth: A stationary wave teleconnection mechanism and implications for the South Asian monsoons. *J. Climate*, **18**, 2067–2079, <https://doi.org/10.1175/JCLI3391.1>.
- Shao, Q., W. Cao, J. Fan, L. Huang, and X. Xu, 2017: Effects of an ecological conservation and restoration project in the Three-River Source Region, China. *J. Geogr. Sci.*, **27**, 183–204, <https://doi.org/10.1007/s11442-017-1371-y>.
- Shen, M., Y. Tang, J. Chen, X. Zhu, and Y. Zheng, 2011: Influences of temperature and precipitation before the growing season on spring phenology in grasslands of the central and eastern Qinghai-Tibetan Plateau. *Agric. For. Meteor.*, **151**, 1711–1722, <https://doi.org/10.1016/j.agrformet.2011.07.003>.
- Shi, H., T. Li, J. Wei, W. Fu, and G. Wang, 2016: Spatial and temporal characteristics of precipitation over the Three-River Headwaters region during 1961–2014. *J. Hydrol. Reg. Stud.*, **6**, 52–65, <https://doi.org/10.1016/j.ejrh.2016.03.001>.
- Simmonds, I., D. Bi, and P. Hope, 1999: Atmospheric water vapor flux and its association with rainfall over China in summer. *J. Climate*, **12**, 1353–1367, [https://doi.org/10.1175/1520-0442\(1999\)012<1353:AWVFAI>2.0.CO;2](https://doi.org/10.1175/1520-0442(1999)012<1353:AWVFAI>2.0.CO;2).
- Sohn, B. J., S. W. Yeh, J. Schmetz, and H. J. Song, 2013: Observational evidences of Walker circulation change over the last 30 years contrasting with GCM results. *Climate Dyn.*, **40**, 1721–1732, <https://doi.org/10.1007/s00382-012-1484-z>.
- Sugimoto, S., and K. Ueno, 2010: Formation of mesoscale convective systems over the eastern Tibetan Plateau affected by plateau-scale heating contrasts. *J. Geophys. Res.*, **115**, D16105, <https://doi.org/10.1029/2009JD013609>.
- Sun, B., and H. Wang, 2018: Interannual variation of the spring and summer precipitation over the Three River Source region in China and the associated regimes. *J. Climate*, **31**, 7441–7457, <https://doi.org/10.1175/JCLI-D-17-0680.1>.
- , —, and —, 2019: Enhanced connections between summer precipitation over the Three-River-Source region of China and the global climate system. *Climate Dyn.*, **52**, 3471–3488, <https://doi.org/10.1007/s00382-018-4326-9>.
- Sun, J., K. Yang, W. Guo, Y. Wang, J. He, and H. Lu, 2020: Why has the inner Tibetan Plateau become wetter since the mid-1990s? *J. Climate*, **33**, 8507–8522, <https://doi.org/10.1175/JCLI-D-19-0471.1>.
- Tong, K., F. Su, D. Yang, L. Zhang, and Z. Hao, 2014: Tibetan Plateau precipitation as depicted by gauge observations, reanalyses and satellite retrievals. *Int. J. Climatol.*, **34**, 265–285, <https://doi.org/10.1002/joc.3682>.
- Tong, L., X. Xu, Y. Fu, and S. Li, 2014: Wetland changes and their responses to climate change in the “Three-River Headwaters” region of China since the 1990s. *Energies*, **7**, 2515–2534, <https://doi.org/10.3390/en7042515>.
- Trenberth, K. E., and D. P. Stepaniak, 2001: Indices of El Niño evolution. *J. Climate*, **14**, 1697–1701, [https://doi.org/10.1175/1520-0442\(2001\)014<1697:LIOENO>2.0.CO;2](https://doi.org/10.1175/1520-0442(2001)014<1697:LIOENO>2.0.CO;2).
- Wang, C., and Y. Guo, 2012: Precipitable water conversion rates over the Qinghai-Xizang (Tibet) Plateau: Changing characteristics with global warming. *Hydrol. Processes*, **26**, 1509–1516 <https://doi.org/10.1002/hyp.8246>.

- , W. Dong, and Z. Wei, 2002: Anomaly feature of seasonal frozen soil variations on the Qinghai-Tibet Plateau. *J. Geogr. Sci.*, **12**, 99–107, <https://doi.org/10.1007/BF02837433>.
- Wang, Z., A. Duan, S. Yang, and K. Ullah, 2017: Atmospheric moisture budget and its regulation on the variability of summer precipitation over the Tibetan Plateau. *J. Geophys. Res.*, **122**, 614–630, <https://doi.org/10.1002/2016JD025515>.
- , R. Wu, P. Zhao, S. L. Yao, and X. Jia, 2019: Formation of snow cover anomalies over the Tibetan Plateau in cold seasons. *J. Geophys. Res.*, **124**, 4873–4890, <https://doi.org/10.1029/2018JD029525>.
- Webster, P. J., 2004: The elementary Hadley circulation. *The Hadley Circulation: Past, Present and Future*, H. Diaz and R. Bradley, Eds., Cambridge University Press, 9–60.
- Wei, J., H. R. Knoche, and H. Kunstmann, 2015: Contribution of transpiration and evaporation to precipitation: An ET-tagging study for the Poyang Lake region in Southeast China. *J. Geophys. Res.*, **120**, 6845–6864, <https://doi.org/10.1002/2014JD022975>.
- Wu, J., and X. J. Gao, 2013: A gridded daily observation dataset over China region and comparison with the other datasets. *Chin. J. Geophys.*, **56**, 1102–1111, <https://doi.org/10.6038/cjg20130406>.
- Wu, M., T. Zhou, X. Chen, and B. Wu, 2020: Intermodel uncertainty in the projection of the anomalous western North Pacific anticyclone associated with El Niño under global warming. *Geophys. Res. Lett.*, **47**, e2019GL086139, <https://doi.org/10.1029/2019GL086139>.
- Wu, Q., and T. Zhang, 2008: Recent permafrost warming on the Qinghai-Tibetan Plateau. *J. Geophys. Res.*, **113**, D13108, <https://doi.org/10.1029/2007JD009539>.
- Wu, R., I. L. Kinter, and B. P. Kirtman, 2005: Discrepancy of interdecadal changes in the Asian region among the NCEP–NCAR reanalysis, objective analyses, and observations. *J. Climate*, **18**, 3048–3067, <https://doi.org/10.1175/JCLI3465.1>.
- Xi, Y., C. Miao, J. Wu, Q. Duan, X. Lei, and H. Li, 2018: Spatiotemporal changes in extreme temperature and precipitation events in the Three-Rivers Headwater region, China. *J. Geophys. Res.*, **123**, 5827–5844, <https://doi.org/10.1029/2017JD028226>.
- Xu, M., S. Kang, Q. Zhao, and J. Li, 2016: Terrestrial water storage changes of permafrost in the three-river source region of the Tibetan Plateau, China. *Adv. Meteor.*, **2016**, 4364738, <https://doi.org/10.1155/2016/4364738>.
- , —, X. Chen, H. Wu, X. Wang, and Z. Su, 2018: Detection of hydrological variations and their impacts on vegetation from multiple satellite observations in the Three-River Source Region of the Tibetan Plateau. *Sci. Total Environ.*, **639**, 1220–1232, <https://doi.org/10.1016/j.scitotenv.2018.05.226>.
- Xu, X., C. Lu, X. Shi, and S. Gao, 2008: World water tower: An atmospheric perspective. *Geophys. Res. Lett.*, **35**, L20815, <https://doi.org/10.1029/2008GL035867>.
- Xu, Z. X., T. L. Gong, and J. Y. Li, 2008: Decadal trend of climate in the Tibetan Plateau—Regional temperature and precipitation. *Hydrol. Processes*, **22**, 3056–3065, <https://doi.org/10.1002/hyp.6892>.
- Yanai, M., and T. Tomita, 1998: Seasonal and interannual variability of atmospheric heat sources and moisture sinks as determined from NCEP–NCAR reanalysis. *J. Climate*, **11**, 463–482, [https://doi.org/10.1175/1520-0442\(1998\)011<0463:SAIVOA>2.0.CO;2](https://doi.org/10.1175/1520-0442(1998)011<0463:SAIVOA>2.0.CO;2).
- Yang, K., H. Wu, J. Qin, C. Lin, W. Tang, and Y. Chen, 2014: Recent climate changes over the Tibetan Plateau and their impacts on energy and water cycle: A review. *Global Planet. Change*, **112**, 79–91, <https://doi.org/10.1016/j.gloplacha.2013.12.001>.
- Yang, S., K. M. Lau, and K. M. Kim, 2002: Variations of the East Asian jet stream and Asian-Pacific-American winter climate anomalies. *J. Climate*, **15**, 306–325, [https://doi.org/10.1175/1520-0442\(2002\)015<0306:VOTEAJ>2.0.CO;2](https://doi.org/10.1175/1520-0442(2002)015<0306:VOTEAJ>2.0.CO;2).
- Yao, T., and Coauthors, 2012: Different glacier status with atmospheric circulations in Tibetan Plateau and surroundings. *Nat. Climate Change*, **2**, 663–667, <https://doi.org/10.1038/nclimate1580>.
- Yi, X., G. Li, and Y. Yin, 2013: Spatio-temporal variation of precipitation in the Three-River Headwater Region from 1961 to 2010. *J. Geogr. Sci.*, **23**, 447–464, <https://doi.org/10.1007/s11442-013-1021-y>.
- You, Q., J. Min, Y. Jiao, M. Sillanpää, and S. Kang, 2016: Observed trend of diurnal temperature range in the Tibetan Plateau in recent decades. *Int. J. Climatol.*, **36**, 2633–2643, <https://doi.org/10.1002/joc.4517>.
- , and Coauthors, 2020: Review of snow cover variation over the Tibetan Plateau and its influence on the broad climate system. *Earth-Sci. Rev.*, **201**, 103043, <https://doi.org/10.1016/j.earscirev.2019.103043>.
- Zhang, C., and P. J. Webster, 1989: Effects of zonal flows on equatorially trapped waves. *J. Atmos. Sci.*, **46**, 3632–3652, [https://doi.org/10.1175/1520-0469\(1989\)046<3632:EOZFOE>2.0.CO;2](https://doi.org/10.1175/1520-0469(1989)046<3632:EOZFOE>2.0.CO;2).
- Zhang, L., F. Su, D. Yang, Z. Hao, and K. Tong, 2013: Discharge regime and simulation for the upstream of major rivers over Tibetan Plateau. *J. Geophys. Res. Atmos.*, **118**, 8500–8518, <https://doi.org/10.1002/jgrd.50665>.
- Zhang, Y., S. Zhang, X. Zhai, and J. Xia, 2012: Runoff variation and its response to climate change in the Three Rivers Source Region. *J. Geogr. Sci.*, **22**, 781–794, <https://doi.org/10.1007/s11442-012-0963-9>.
- Zhang, Z., J. Arnault, S. Wagner, P. Laux, and H. Kunstmann, 2019: Impact of lateral terrestrial water flow on land–atmosphere interactions in the Heihe river basin in China: Fully coupled modeling and precipitation recycling analysis. *J. Geophys. Res.*, **124**, 8401–8423, <https://doi.org/10.1029/2018JD030174>.
- Zhao, P., Z. Zhou, and J. Liu, 2007: Variability of Tibetan spring snow and its associations with the hemispheric extratropical circulation and East Asian summer monsoon rainfall: An observational investigation. *J. Climate*, **20**, 3942–3955, <https://doi.org/10.1175/JCLI4205.1>.
- Zheng, Y., J. Han, Y. Huang, S. R. Fassnacht, S. Xie, E. Lv, and M. Chen, 2018: Vegetation response to climate conditions based on NDVI simulations using stepwise cluster analysis for the Three-River Headwaters region of China. *Ecol. Indic.*, **92**, 18–29, <https://doi.org/10.1016/j.ecolind.2017.06.040>.
- Zhou, B., Y. Xu, J. Wu, S. Dong, and Y. Shi, 2016: Changes in temperature and precipitation extreme indices over China: Analysis of a high-resolution grid dataset. *Int. J. Climatol.*, **36**, 1051–1066, <https://doi.org/10.1002/joc.4400>.
- Zhou, C., P. Zhao, and J. Chen, 2019: The interdecadal change of summer water vapor over the Tibetan Plateau and associated mechanisms. *J. Climate*, **32**, 4103–4119, <https://doi.org/10.1175/JCLI-D-18-0364.1>.
- Zhu, J., Y. Zhou, S. Wang, L. Wang, F. Wang, W. Liu, and B. Guo, 2015: Multicriteria decision analysis for monitoring ecosystem service function of the Three-River Headwaters region of the Qinghai-Tibet Plateau, China. *Environ. Monit. Assess.*, **187**, 355, <https://doi.org/10.1007/s10661-015-4523-5>.